Ground and Lower Excited States of Methyl Peroxy, CH_3O_2, Radical: A Computational Investigation†

Jawed A. Jafri and Donald H. Phillips*

Contribution from the NASA Langley Research Center, Hampton, Virginia 23665.
Received February 13, 1989

Abstract: The ground and lower excited states of methyl peroxy, CH_3O_2, radical have been investigated at the selected pseudo-first-order configuration interaction (CI) level by use of a double-ζ basis set. Selected singles and doubles CI calculations using a polarized double-ζ basis have been carried out on the two lowest states in the A'' symmetry. Dissociation energies with respect to $CH_3O_2 \rightarrow CH_3 + O_2$ and $CH_3O + O$ are computed to be 2.01 and 3.37 eV, respectively, The observed absorption in the vicinity of 240 nm is assigned to the $X^2A'' \rightarrow 2^2A''$ transition. Channels to both $CH_3O + O$ and $CH_3 + O + O$ photolysis products are found to be open. Curve crossings between various states and photodissociation products are discussed and the dipole moment along various slices through the potential energy surface is evaluated.

The methyl peroxy radical, CH_3O_2, is an important intermediate in combustion processes[1] and in the reaction of methane in the troposphere and stratosphere,[2] resulting in the production or destruction of ozone. The fractional abundance of CH_3O_2 radical in the troposphere is estimated at 10^{-11} with a lifetime of 10^3 s.[3,4] Its role in the chain reactions

$$CH_4 + OH \rightarrow CH_3 + H_2O \quad (1)$$

$$CH_3 + O_2 + M \rightarrow CH_3O_2 + M \quad (2)$$

$$CH_3O_2 + NO \rightarrow CH_3O + NO_2 \quad (3)$$

$$CH_3O + O_2 \rightarrow H_2CO + HO_2 \quad (4)$$

$$HO_2 + NO \rightarrow OH + NO_2 \quad (5)$$

$$2(NO_2 + h\nu \rightarrow NO + O) \quad (6)$$

$$2(O + O_2 + M \rightarrow O_3 + M) \quad (7)$$

$$\text{net reaction} \quad CH_4 + 4O_2 \rightarrow H_2O + H_2CO + 2O_3 \quad (8)$$

may contribute to ozone generation in the presence of high atmospheric NO_x concentration.[5] The production of H_2CO and other reactions of CH_3O_2 are also of importance in the trace-gas chemistry of the atmosphere.

A large fraction of mutual interactions of methyl peroxy radicals

$$2CH_3OO \rightarrow 2CH_3O + O_2$$

$$CH_3O + O_2 \rightarrow HCHO + HO_2$$

are nonterminating, generating HO_2 and CH_3O radicals, which in turn react with CH_3O_2 in a complex manner,[6] A fraction of each of these daughter radicals consume methyl peroxy radicals by

$$CH_3OO + CH_3O \rightarrow CH_3OOH + HCHO$$

$$CH_3OO + HOO \rightarrow CH_3OOH + O_2$$

The absorption spectrum of methyl peroxy radical in the gas phase has been described by Parkes and co-workers,[7-9] by Hochandel et al.,[10] and by Calvert and co-workers[11,12] and consists of a broad, structureless, and comparatively weak band. These sources, however, differ somewhat in their quantitative characterization of the absorption maximum. Adachi, Basco, and James[6] have characterized the absorption spectrum of CH_3O_2 as a weak, broad, structureless band having a maximum at 240 nm with a decadic extinction coefficient of $\epsilon(240) = 1.55 \times 10^3$ L/mol cm, Electronic absorption spectra of CH_3O_2 and several other peroxy radicals have been reported in the near-infrared (1.0–1.6 nm),[13] with the value for $X^2A'' \rightarrow 1^2A'$ transition at 0.914 eV. The rates of reaction of CH_3O_2 with several other trace-gas species have been reported in recent years,[6,12,14] The nature of photolysis products, however, was not determined in the absorption experiments and the heat of formation of CH_3O_2 is subject to considerable uncertainty.

Bair and Goddard[15] studied the ground state of CH_3O_2 to determine the equilibrium geometry using a valence double-ζ basis set augmented by polarization functions in a generalized valence bond–configuration interaction (GVB–CI)[18] scheme. Besler et al.[16] calculated the ground-state geometry and other properties of a series of hydrocarbon peroxy radicals using a large basis set at UHF and Møeller–Plesset perturbation theory to the second order,[17] These computations, however, did not determine the dissociation energy or the nature of the excited states, In this work, we attempt to calculate the ground-state equilibrium geometry, the dissociation energies with respect to various fragments, the nature of excited states, and photolysis products using a good basis set and the configuration interaction method,

Computational Methods

Two sets of computations were carried out to study the ground and excited states of CH_3O_2 radical. The first set of computations utilized methods designed to yield qualitative accuracy. These calculations were used to scan the potential energy surfaces of several of the lower energy states of CH_3O_2. In these calculations the molecular orbitals were obtained by using the GVB(PP) method[18] and an atomic basis set of dou-

†Support for J.A.J. under NASA Grant NAG-1-596 to the Chemical Sciences Department of Old Dominion University is gratefully acknowledged.

(1) Benson, S. W.; Nangia, P. S. *Acc. Chem. Res.* **1979**, *12*, 223.
(2) Heiklen, J. *Atmospheric Chemistry*; Academic Press: New York, 1977.
(3) Pitts, J. N. *NASA Ref. Publ. 1022* **1978**, 53.
(4) Drakes, D. A.; Paul, D. M.; Quinn, G. P.; Robson, R. C. *Chem. Phys. Lett.* **1973**, *23*, 425.
(5) Lin, S. C. *NASA Ref. Publ. 1022* **1978**, 65–79.
(6) Adachi, H.; Basco, N.; James, G. L. *Int. J. Chem. Kinet.* **1980**, *12*, 949.
(7) Parkes, D. A. In *Proceedings of the 15th Symposium on Combustion* (Tokyo, 1974); Combustion Institute: Pittsburgh, PA, 1975; p 795.
(8) Parkes, D. A. *Int. J. Chem. Kinet.* **1977**, *9*, 451.
(9) Anastasi, C.; Smith, I. W. M.; Parkes, D. A. *J. Chem. Soc., Faraday Trans. 1* **1978**, *74*, 1693.
(10) Hochandel, C. J.; Ghormley, J. A.; Boyle, J. W.; Ogren, P. J. *J. Chem. Phys.* **1977**, *81*, 3.
(11) Kan, C. S.; Calvert, G. S. *Chem. Phys. Lett.* **1979**, *63*, 111.
(12) Kan, C. S.; McQuigg, R. D.; Whitebeck, M. R.; Calvert, J. G. *Int. J. Chem. Kinet.* **1979**, *11*, 921.
(13) Hunziker, H. E.; Wendt, H. R. *J. Chem. Phys.* **1976**, *64*, 3488.
(14) Sanhueza, E.; Simonaitis, R.; Heiklen, J. *Int. J. Chem. Kinet.* **1979**, *11*, 907.
(15) Bair, R. A.; Goddard, W. A. *J. Am. Chem. Soc.* **1982**, *104*, 2719.
(16) Besler, B. M.; Sevilla, M. D.; MacNeille, P. *J. Phys. Chem.* **1986**, *90*, 6446.
(17) Pople, J. A.; Binkley, J. S.; Seger, R. *Int. J. Quantum Chem.* **1976**, *S10*, 1. Binkley, J. S.; Pople, J. A. *Ibid.* **1975**, *9*, 229. Krishnan, R.; Pople, J. A. *Ibid.* **1978**, *14*, 91. Pople, J. A.; Schlegel, H. B.; Binkley, J. S. *Ibid.* **1979**, *S13*, 225.

0002-7863/90/1512-2586$02.50/0

Table I. PFO CI Results for the O–O Coordinate in CH_3O_2 (C–O Distance Fixed at 2.75 Bohr)

R_{OO}, bohr	state	E_1[a]	E_2[a]	E_3[a]
2.1505	A″	−189.298021	−188.984950	−188.927101
	A′	−189.239457	−188.974894	−188.068584
2.430	A″	−189.366776	−189.137986	−189.006940
	A′	−189.323150	−189.108858	−189.051324
2.530	A″	−189.375718	−189.172388	−189.060038
	A′	−189.336555	−189.137441	−189.102755
2.680	A″	−189.380272	−189.209729	−189.121958
	A′	−189.347146	−189.167850	−189.161750
2.783	A″	−189.379000	−189.227709	−189.153899
	A′	−189.349894	−189.191495	−189.182926
2.900	A″	−189.375016	−189.242442	−189.181881
	A′	−189.349249	−189.217065	−189.194490
3.036	A″	−189.368279	−189.253157	−189.205724
	A′	−189.347488	−189.239335	−189.203314
3.289	A″	−189.353644	−189.260269	−189.230523
	A′	−189.339151	−189.264805	−189.212428
3.610	A″	−189.336507	−189.267475	−189.251220
	A′	−189.327569	−189.281986	−189.217849
3.790	A″	−189.329485	−189.264481	−189.252198
	A′	−189.324086	−189.288061	−189.216604
500.00	A″	−189.309762	−189.295345	−189.224714
	A′	−189.304290	−189.302305	−189.216360

[a] E_1, E_2, and E_3 represent the lowest three roots of CH_3O_2 in each symmetry. Values in hartrees.

ble-ζ quality.[19,20] The CI wave function used was an approximation to the first-order wave function.[21] Perturbation theory[22] was utilized to select final configurations from an initial list that contained all double excitations in the valence space and all single excitations in the virtual space relative to a set of important configurations. These calculations will be referred to as pseudo-first-order (PFO) CI.

The second set of computations, which utilized methods designed to produce quantitative accuracy, was used to investigate the two states deemed likely to be of importance to the atmospheric chemistry of CH_3O_2 on the basis of the first set of computations. In order to obtain this accuracy, several improvements were made in the computational procedures: (a) the atomic basis sets were augmented with polarization functions on all atoms;[23] (b) approximate natural orbitals (ANOs)[22a] were obtained for each state by carrying out limited CI calculations; and (c) double excitations into the virtual space were permitted in the initial list of CI configurations. Perturbation theory selection of the final set of configurations was utilized in this set of calculations also. This wave function is an approximation to the second-order CI[24] and in parallel with the first set will be referred to as pseudo-second-order (PSO) CI. These calculations are also similar to those shown by Bauschlicher et al.[25] to yield results that exhibit good agreement with full CI calculations. The primary remaining source of error arises from the incompleteness of the basis set used in the calculations. Pople et al.[26] have recently reported an extensive set of basis set errors for the 6-311G** bases. The latter are of a quality similar to those utilized here. The differences between the basis errors for H_3COH and those for fragment sets like $H_2CO + H_2$, $H_2O + H_2C$, and $H_3C + OH$ were found to range between ~1.8 and 4 kcal/mol. A similar basis set error range is expected for the present calculations.

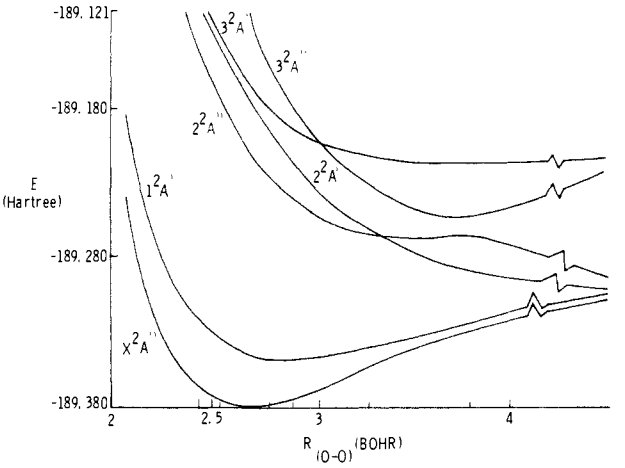

Figure 1. Pseudo-first-order CI energies of the lower $^2A''$ and $^2A'$ states of CH_3O_2 as a function of R_{OO}.

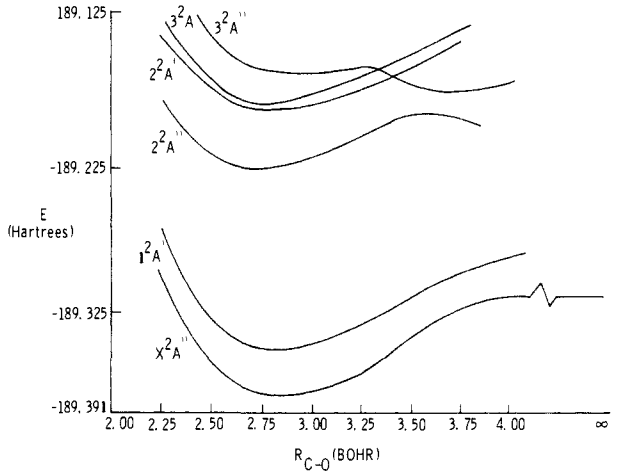

Figure 2. Pseudo-first-order CI energies of the lower $^2A''$ and $^2A'$ states of CH_3O_2 as a function of R_{CO}.

Table II. PFO CI Results for the C–O Coordinate in CH_3O_2 (O–O Distance Fixed at 2.783 Bohr)

R_{CO}, bohr	state	E_1[a]	E_2[a]	E_3[a]
2.4425	A″	−189.350966	−189.213618	−189.120739
	A′	−189.321927	−189.165722	−189.161895
2.600	A″	−189.371913	−189.226331	−189.151162
	A′	−189.342519	−189.183436	−189.179728
2.725	A″	−189.379219	−189.228451	−189.158422
	A′	−189.349362	−189.190420	−189.183653
2.850	A″	−189.380861	−189.226953	−189.160862
	A′	−189.350579	−189.191848	−189.183186
2.998	A″	−189.378283	−189.221670	−189.159368
	A′	−189.347174	−189.188517	−189.178544
3.270	A″	−189.365512	−189.207281	−189.154780
	A′	−189.332228	−189.175355	−189.164866
3.543	A″	−189.347680	−189.191854	−189.168344
	A′	−189.312382	−189.156824	−189.147050
3.815	A″	−189.329582	−189.200697	−189.172280
	A′	−189.294127	−189.164362	−189.130020
500.00[b]	A″	−189.315773	−189.089019	−188.981690

[a] E_1, E_2, and E_3 refer to the lowest three roots of CH_3O_2 in each symmetry. Values in hartrees. [b] The orbitals for CH_3O_2 radical were computed in $^4A''$ state at this geometry.

The CH_3 group in CH_3O_2 radical was held at fixed geometry in all calculations. The CH bonds were 1.04 Å and the HCH angles were 109°. The COO angles was also frozen at 110° in the same plane as one hydrogen, while the other two hydrogen atoms were above and below this plane. These structural parameters are similar to those of Besler, Sevilla, and MacNeille, who found nearly degenerate cis and trans structures for the ground state.[16] At infinite separation of $CH_3O + O$, however, the COO angle was relaxed to 180°, and the CH_3O geometry determined

(18) Hunt, W. J.; Hay, P. J.; Goddard, W. A. *J. Chem. Phys.* **1972**, *57*, 738. Barbowicz, F. W.; Goddard, W. A. In *Modern Theoretical Chemistry*; Schaefer, H. F., III, Eds.; Plenum Press: New York, 1977; Vol. III, pp 79–127.
(19) Dunning, T. H. *J. Chem. Phys.* **1970**, *53*, 2823.
(20) Huzinaga, S. *J. Chem. Phys.* **1965**, *42*, 1293.
(21) Schaefer, H. F.; Harris, F. E. *Phys. Rev. Lett.* **1968**, *21*, 1561.
(22) Shavitt, I. In *Modern Theoretical Chemistry*; Schaefer, H. F., III, Ed.; Plenum Press: New York, 1977; Vol. III. Gershgorn, Z.; Shavitt, I. *Int. J. Quantum Chem.* **1961**, *2*, 751. Bernal, M. J. M.; Boys, S. F. *Philos. Trans. R. Soc. London, A* **1952**, *No. 245*, 139. Raffenetti, R. C.; Hsu, K.; Shavitt, I. *Theor. Chim. Acta* **1977**, *45*, 33.
(23) Dunning, T. H.; Hay, P. J. In *Modern Theoretical Chemistry*; Schaefer, H. F., III, Ed.; Plenum Press: New York, 1977; Vol. III.
(24) Mulliken, R. S.; Ermler, W. C. *Polyatomic Molecules*; Academic Press: 1981; p 30.
(25) Bauschlicher, C. W.; Taylor, P. R. *J. Chem. Phys.* **1987**, *86*, 1420, and refs 4–9 therein.
(26) Pople, J. A.; Head-Gordon, M.; Fox, D. J.; Raghavachari, K.; Curtiss, L. A. *J. Chem. Phys.* **1989**, *90*, 5622.

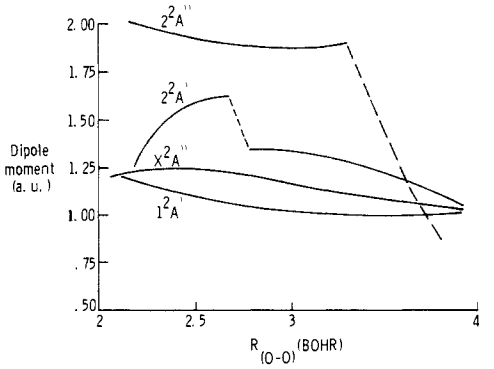

Figure 3. Pseudo-first-order Cl dipole moment of the two lowest $^2A''$ and $^2A'$ states of CH_3O_2 as a function of R_{OO}.

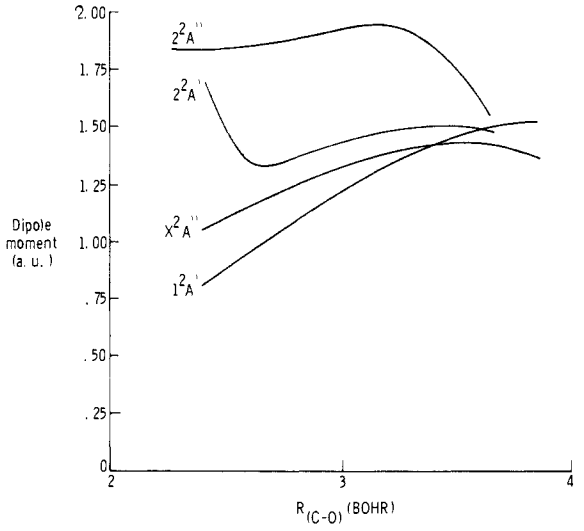

Figure 4. Pseudo-first-order CI dipole moment of the two lowest $^2A''$ and $^2A'$ states of CH_3O_2 as a function of R_{CO}.

by Jackels[27] was used, i.e., R_{CO} = 1.614 Å, R_{CH} = 1.091 Å, θ_{HCO} = 102.6°, θ_{HCH} = 109°. R_{OO} was optimized at the infinite separate configuration $CH_3 + O_2$ at 1.244 Å. A more detailed description of the calculational methods is submitted as supplementary material.

Results

A. PFO Results. Slices through the potential energy surfaces for the three lowest $^2A''$ and $^2A'$ states where the R_{OO} was varied holding the R_{CO} fixed at 2.725 bohr are plotted in Figure 1 and presented in Table I. The energies of the three lowest $^2A''$ and $^2A'$ states as a function of the R_{CO}, holding R_{OO} fixed at 2.783 bohr, are presented in Table II and plotted in Figure 2. The dipole moment curves for the two lowest lying states in $^2A''$ and $^2A'$ symmetries along the O–O coordinate are plotted in Figure 3 and those along the C–O coordinate in Figure 4.

1. A″ States. Along the C–O coordinate, the first excited state in the $^2A''$ symmetry (Figure 2) exhibits a bound region with a minimum near R_{CO} = 2.75 bohr and an avoided crossing with the third $^2A''$ state near R_{CO} = 3.6 bohr. Along the O–O coordinate, (Figure 1), the first excited state is essentially repulsive near R_{OO} = 2.75 bohr but exhibits very slight binding near R_{OO} = 3,30 bohr and an avoided crossing with the third $^2A''$ state near R_{OO} = 3,80 bohr.

The dissociation energies at this level of treatment are

$$D(CH_3O_2 \rightarrow CH_3 + O_2) = 1.771 \text{ eV}$$

$$D(CH_3O_2 \rightarrow CH_3O + O) = 1,919 \text{ eV}$$

2. A′ States. The first $^2A'$ state is bound along both the O–O and C–O stretching coordinates, as expected on the basis of spectroscopic investigations of CH_3O_2 absorption in the near-infrared. The second and third $^2A'$ states are bound near R_{CO} = 2.75 bohr (Figure 2) along the C–O coordinate and are repulsive along the O–O coordinate, Both of these states exhibit a crossing with the third $^2A''$ state on the C–O coordinate at ~3,3 bohr. The excitation energy at this level of computation is

$$X^2A'' \rightarrow 1^2A' = 0.901 \text{ eV}$$

The $2^2A'$ state crosses the $2^2A''$ state in the region where the PFO CI results indicate that the latter may be slightly bound.

The dipole moment functions (DMFs) for the CH_3O_2 in the O–O and C–O coordinates are plotted in Figures 3 and 4, respectively, at the PFO CI level of computation. The DMFs for the ground state (X^2A'') and for the lowest state in the $^2A'$ symmetry vary smoothly with respect to the respective changes in the coordinates. The DMFs for the first excited state in both symmetries, however, show discontinuities due to curve crossing in the O–O coordinate near 2,8 bohr for the $^2A'$ and 3.7 bohr for the $^2A''$ symmetry, Similar behavior is observed for the DMF of the $2^2A''$ state in the C–O coordinate, with the avoided curve crossing in the vicinity of 3.5 bohr.

B. PSO CI Results. A second series of calculations was carried out on the lowest two states of CH_3O_2 in the A″ symmetry along the C–O coordinate with fixed O–O distance and along the O–O coordinate at fixed C–O distance to obtain a more accurate description of these states. The equilibrium geometry, dissociation energy, and any binding in the second $^2A''$ state was explored by use of a polarized DZ basis set and PSO CI as discussed under Computational Methods. These calculations utilized approximate natural orbitals obtained from a small CI calculation for each state treated. The energies for the first two $^2A''$ states along the O–O coordinate, where the C–O bond length was fixed at 2.75 bohr, are presented in Table III and plotted in Figure 5. The second $^2A''$ state exhibits slight binding similar to that found in the PFO results except that the minimum is found to be near 3.0 bohr. The dissociation energy for the $CH_3O_2 \rightarrow CH_3O + O$ at the higher level of treatment is predicted to be at 3.365 eV, a significant increase over that predicted at the PFO CI level.

The refined calculations along the C–O coordinate, with R_{OO} fixed at 2.56 bohr, are plotted in Figure 6 and presented in Table IV. These computations produce results very similar to the ones using the PFO procedure. The avoided crossing between the $2^2A''$

Table III. PSO CI Energies of the X^2A'' and $2^2A''$ States along the O–O Coordinate with R_{CO} = 2.748 Bohr)

R_{OO}, bohr	X^2A''[a]	$2^2A''$[a]
2.411	−189.627009	−189.360728
2.56	−189.634754	−189.399470
2.71	−189.629232	−189.429652
2.80	−189.624619	−189.438978
2.86	−189.619795	−189.460298
3.00	−189.609292	−189.448384
3.30	−189.583719	−189.476526
3.80	−189.554940	−189.444410
500.00[b]	−189.511096	

[a] Values in hartrees. [b] R_{CO} = 2.649 bohr. See text for details of geometry.

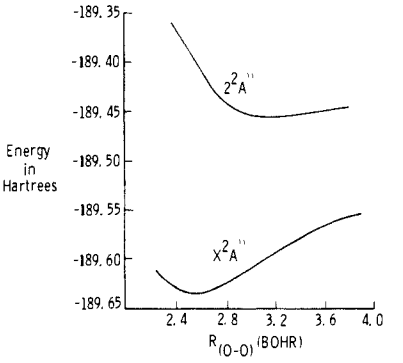

Figure 5. Pseudo-second-order CI energies of the two lowest $^2A''$ states of CH_3O_2 as a function of R_{OO}.

(27) Jackels, C. F. *J. Chem. Phys.* **1985**, *82*, 311.

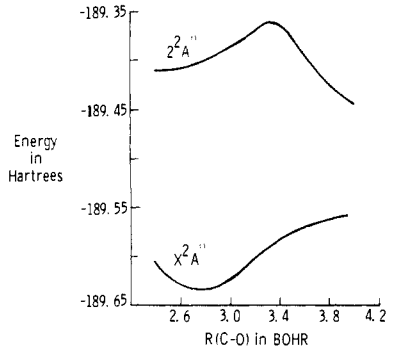

Figure 6. Pseudo-second-order CI energies of the two lowest $^2A''$ states of CH_3O_2 as a function of R_{CO}.

Table IV. PSO CI Energies for the X^2A'' and $2^2A''$ States along the C–O Coordinate (R_{OO} Fixed at 2.56 Bohr)[a]

R_{CO}, bohr	X^2A''[b]	$2^2A''$[b]
2.598	-189.631742	-189.408465
2.748	-189.634754	-189.399470
2.898	-189.629929	-189.395334
3.100	-189.615957	-189.380685
3.300	-189.587609	-189.363211
3.600	-189.575821	-189.402720
3.900	-189.556006	-189.438198
500.00[c]	-189.560815	

[a] Both states employed their own approximate natural orbitals calculated separately. [b] Values in hartrees. [c] The COO angle was changed to 180° and the R_{OO} was optimized at 2.35 bohr for this geometry.

Table V. PSO CI Energies for the X^2A'' and $2^2A''$ States along the Coordinate Defined by the 45° Angle through the Plane Defined by R_{CO} and R_{OO} Stretches[a]

R, bohr	X^2A''[b]	$2^2A''$[b]
3.5443	-189.627012	-189.363965
3.6033	-189.632922	-189.380388
3.7583	-189.634754	-189.399470
3.9133	-189.632372	-189.415834
3.968	-189.626890	-189.422632
4.1803	-189.606836	-189.425222

[a] Treatment employed approximate natural orbitals, which were calculated separately for each state. [b] Values in hartrees.

and $3^2A''$ states is near $R_{CO} = 3.2$ bohr. The dissociation energy for $CH_3O_2 \rightarrow CH_3 + O_2$ at this level of computation is predicted to be 2.012 eV, which is also significantly larger than that obtained with the smaller treatment.

The potential energy curve along a 45° angle in the plane defined by the R_{CO} and R_{OO} coordinates is presented in Table V and plotted in Figure 7. Both the C–O and O–O bonds are broken along this coordinate and the products are CH_3 and two oxygen atoms. In this calculation, as in the previous one, separate ANOs were used for the ground and the first excited state in the $^2A''$ symmetry. The second $^2A''$ state is purely repulsive on this coordinate.

Discussion

The O–O and C–O bonds in the CH_3O_2 radical were optimized separately, while the other bonds and angles were held fixed. This produced, at the PSO CI level, equilibrium values of R_{CO} and R_{OO} equal to 2.748 and 2.561 bohr, respectively, in good agreement with other theoretical values.[15,16] The dissociation energy of $CH_3O_2 \rightarrow CH_3O + O$ computed by using ANOs with DZP basis set and PSO CI procedure is 3.365 eV. The only D_e value for the CH_3O_2 dissociating to these fragments in the literature for comparison is 2.08 eV.[28] This value is calculated from the heat

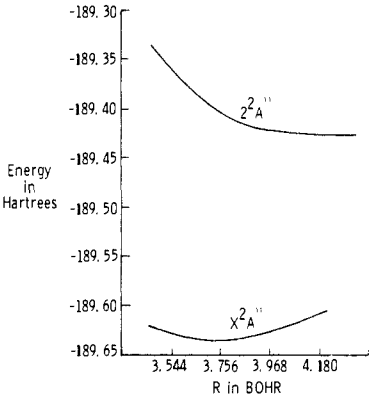

Figure 7. Pseudo-second-order CI energies of the two lowest $^2A''$ states of CH_3O_2 as a function of $R = [R_{CO}^2 + R_{OO}^2]^{1/2}$.

of formation and is not very reliable. This D_e for the O–O bond in the CH_3O_2 radical can be compared to D_e for the O–O fragment in the ClO_2 and HO_2 molecules, which are 3.46[29] and 2.70 eV,[30] respectively. The present value of 3.365 eV lies closer to the ClO_2 value. The dissociation energy of CH_3O_2 to $CH_3 + O_2$ in the present work is 2.012 eV. This is comparable to the OH bond dissociation energy in the HO_2 molecule, which was calculated to be 2.0 eV by Langhoff and Jaffe.[30]

The vertical excitation energy between the $X^2A'' \leftarrow 1^2A'$ is computed to be 0.9 eV in the PFO calculations, in agreement with the experimental value of 0.914 eV.[13]

The vertical excitation energies and shapes of the potential energy curves suggest that only the lowest two states of each symmetry could be of any significance to the photodissociation of CH_3O_2 in the atmosphere. However, the first $^2A'$ state is bound and the excitation energy of $2^2A'$ is high. Thus, atmospheric photodissociation would be significant only for excitations to the $2^2A''$ state.

The factor of (approximately) 2 difference between the DMFs of the X^2A'' and $2^2A''$ states indicates that the transition between these states should be moderately strong due to the charge transfer accompanying excitation. This difference in the DMF between the two states is similar to that calculated for HO_2[30] and the experimental extinction coefficients are of similar size.

The shape of the $2^2A''$ in the O–O coordinate suggests that $CH_3O + O$ would be the principal photolysis products. However, the results for this state along the $R_{CO} = R_{OO}$ slice through the potential energy surface indicates that the channel to $CH_3 + O + O$ may also be open. The calculated energy difference between the X^2A'' and $2^2A''$ states at the PSO CI level corresponds to the position of the observed UV absorption. Photolysis yielding two oxygen atoms, followed by recombination of the methyl radical and each oxygen atom with O_2, forms a catalytic cycle for forming ozone.

$$CH_3O_2 + h\nu \rightarrow CH_3 + O + O$$

$$CH_3 + O_2 \rightarrow CH_3O_2$$

$$2O_2 + 2O \rightarrow 2O_3$$

$$\text{net} \quad 3O_2 + h\nu \rightarrow 2O_3$$

An estimate of the rate of odd oxygen production at most altitudes in the stratosphere by this mechanism indicates that this cycle would not be important relative to odd oxygen production by photolysis of molecular oxygen. It may, however, have some importance in the bottom of the stratosphere and in the upper troposphere where O_2 photolysis is less significant. The importance of the cycle in the latter regions of the atmosphere would depend upon the shape of the long-wavelength tail of the photolysis spectrum. Ozone production by this mechanism may also com-

(28) *Reaction Rate and Photochemical Data for Atmospheric Chemistry*; NBS Special Publication 513; U.S. Department of Commerce: Washington, DC, 1977; p 103.

(29) Jafri, J. A.; Lengsfield, B. H.; Bauschlicher, C. W.; Phillips, D. H. *J. Chem. Phys.* **1985**, *83*, 1693.

(30) Langhoff, S. R.; Jaffe, R. L. *J. Chem. Phys.* **1979**, *71*, 1475.

plicate laboratory photochemistry experiments including hydrocarbons. If the $2^2A''$ state is slightly bound at long O–O bond lengths, a temperature-dependent quantum yield for photolysis could be expected in the long-wavelength tail of the absorption band for this state.

Overall, the lower electronic states of methyl peroxy and resulting molecular properties are similar to those of HO_2, the simplest peroxy compound.

Supplementary Material Available: Detailed description of computational methods (4 pages). Ordering information is given on any current masthead page.

Structure, Bonding, and Dynamics in Heterocyclic Sulfur–Selenium Molecules, Se_xS_y

R. O. Jones* and D. Hohl

Contribution from the Institut für Festkörperforschung, Forschungszentrum Jülich, D-5170 Jülich, Federal Republic of Germany. *Received June 29, 1989*

Abstract: Density functional calculations have been performed for all crown-shaped cyclic isomers of the molecules Se_2S_6, Se_6S_2 (four each), and all cyclic trans isomers of Se_2S_5 and Se_5S_2 (twelve each). The incorporation of molecular dynamics with simulated annealing provides an efficient means for determining the geometries and relative energies and allows the study of structural rearrangements. Even in the low-symmetry molecules Se_xS_y, ground-state energies and the local structure of the energy surface can be determined accurately. The ground states in all molecules have (1,2)-structures, with adjacent minority atoms. In Se_2S_5 we observe a transformation at $T = 300$ K between vicinal (1,2)-conformers. Although the range of energies is very small in each molecule, the ordering of the different structures can be understood in terms of a simple model that allows predictions to be made for other group VIA heterocycles.

I. Introduction

Homocyclic molecules of sulfur (S_n) and selenium (Se_n) are among the best characterized of small atomic clusters. The group VIA elements are unique in that many allotropes comprise regular arrays of ring molecules, and X-ray structure analyses have been performed for S_n (n = 6–8, 10–13, 18, 20)[1,2] and Se_n (n = 6, 8).[1,3] It is natural that mixtures of sulfur and selenium have also received much attention, not only in the vapor phase[4,5] but also as liquids or as solid solutions.[6-8] Most samples prepared in the laboratory comprise a range of molecules, and the characterization of the crystalline phases obtained from the melts has been difficult. The different Se_xS_y species crystallize together, so that the crystal structures reported are disordered, with sulfur and selenium atoms distributed over the atomic sites.[9] The possible complexity is evident from the example of eight-membered rings, where 30 different crown-shaped isomers can occur.

Sulfur and selenium have much in common and it is not surprising that mixed isomers have similar energies and can coexist. The identification and structure of the molecular units in heterocyclic Se–S systems have been the subjects of continuing interest. Apart from the intrinsic interest in the molecules, an understanding of their structures should provide insight into the complex structures of related liquid and amorphous materials, including Se itself. Early kinetic work[4,5] on the molecules was interpreted to exclude the possibility of Se–Se bonds in S_nSe_{8-n} rings, and this was traced[4] to the fact that the Se–Se bond is weaker than both S–S and Se–S bonds. Raman spectroscopy has shown, however, that Se–Se stretching vibrations can readily be identified in such structures,[10] even for mixtures with very low Se concentrations. On the other hand, the S–S stretching band was not seen if the nominal sulfur content dropped below that in Se_6S_2, suggesting that the formation of S–S homonuclear bonds is not favored in mixed crystals with low sulfur content. This apparent asymmetry between S-rich and Se-rich molecules was also attributed to the relative weakness of Se–Se bonds.[10]

The last decade has seen considerable use of Raman spectroscopy to study these systems, with impressive results. The structures of the eight-membered systems 1,2,3-Se_3S_5[11] and 1,2,5,6-Se_4S_4[12] have been determined qualitatively, and the first rings with less than eight atoms [(1,2)-Se_2S_5 and SeS_5] have been prepared and characterized.[13] Ring molecules with a majority of Se atoms (Se_5S, Se_5S_2, Se_6S_2)[14] have also been studied. A comparison with Urey-Bradley force-field calculations of fundamental vibration frequencies of six- and seven-membered Se–S heterocycles[15] showed that the ground state of the last of these contained adjacent Se atoms. ^{77}Se NMR spectroscopy has been used recently[16] to identify isomers of Se_nS_{8-n} obtained from molten mixtures of the elements. The main components were found to be SeS_7 and (1,2)-Se_2S_6, with smaller amounts of twelve others. For a given chemical composition, isomers with all Se atoms adjacent to each other were the most abundant. In the case of Se_2S_5, the ^{77}Se NMR signal in CS_2 solution has a single peak at room temperature, so that the Se atoms are magnetically equivalent on the NMR time scale.[17] In Se_5S_2, the NMR spectrum shows that there are three sets of nonequivalent Se

(1) Donohue, J. *The Structures of the Elements*; Wiley: New York, 1974; Chapter 9.
(2) Steudel, R. In *Studies in Inorganic Chemistry*; Müller, A., Krebs, B., Eds.; Elsevier: Amsterdam, 1984; Vol. 5, p 3.
(3) Steudel, R.; Strauss, E. M. *Adv. Inorg. Chem. Radiochem.* **1984**, *28*, 135.
(4) Cooper, R.; Culka, J. V. *J. Inorg. Nucl. Chem.* **1967**, *29*, 1217.
(5) Schmidt, M.; Wilhelm, E. *Z. Naturforsch.* **1970**, *25B*, 1348.
(6) Steudel, R.; Laitinen, R. *Top. Curr. Chem.* **1982**, *102*, 177.
(7) Bitterer, H., Ed. *Selenium: Gmelin Handbuch der Anorganischen Chemie*, 8. Aufl., Ergänzungsband B2; Springer: Berlin, 1984.
(8) Steudel, R.; Strauss, E. M. In *The Chemistry of Inorganic Homo- and Heterocycles*; Academic: London, 1987; Vol. 2, p 769.
(9) Laitinen, R.; Niinistö, L.; Steudel, R. *Acta Chem. Scand. A* **1979**, *33*, 737.
(10) Eysel, H. H.; Sunder, S. *Inorg. Chem.* **1979**, *18*, 2626.
(11) Laitinen, R.; Rautenberg, N.; Steidel, J.; Steudel, R. *Z. Anorg. Allg. Chem.* **1982**, *486*, 116.
(12) Giolando, D. M.; Papavassiliou, M.; Pickardt, J.; Rauchfuss, T. B.; Steudel, R. *Inorg. Chem.* **1988**, *27*, 2596.
(13) Steudel, R.; Strauss, E. M. *Angew. Chem.* **1984**, *96*, 356.
(14) Steudel, R.; Papavassiliou, M.; Strauss, E. M.; Laitinen, R. *Angew. Chem.* **1986**, *98*, 81.
(15) Laitinen, R.; Steudel, R.; Strauss, E. M. *J. Chem. Soc. Dalton Trans.* **1985**, 1869.
(16) Laitinen, R. S.; Pakkanen, T. P. *Inorg. Chem.* **1987**, *26*, 2598.
(17) Steudel, R.; Papavassiliou, M.; Jensen, D.; Seppelt, K. *Z. Naturforsch.* **1988**, *43B*, 245.

0002-7863/90/1512-2590$02.50/0